Test and Analysis Correlation of a Large-Scale, Orthogrid-Stiffened Metallic Cylinder without Weld Lands

Michelle T. Rudd[1]
NASA Marshall Space Flight Center, Huntsville, AL, 35812

Mark W. Hilburger [2], Andrew E. Lovejoy[3], Michael C. Lindell[4]
NASA Langley Research Center, Hampton, VA, 23681

Nathaniel W. Gardner[5]
Analytical Services and Materials, Inc., Hampton, VA, 23666

and

Marc R. Schultz[6]
NASA Langley Research Center, Hampton, VA, 23681

Extended Abstract of Proposed Paper for the 59th AIAA/ASME/ASCE/AHS/ASC Structures, Structural Dynamics, and Materials Conference, with AIAA SciTech 2018
January 8-12, 2018
Kissimmee, FL

Category: Structures

Submitted for Inclusion in Special Session: Stability of Structural Shells

Nomenclature

CAD	=	Computer aided design
DIC	=	Digital image correlation
IML	=	Inner mold line
LaRC	=	NASA Langley Research Center
MSFC	=	NASA Marshall Space Flight Center
NESC	=	NASA Engineering and Safety Center
OML	=	Outer mold line
SBKF	=	Shell Buckling Knockdown Factor
STA8.1	=	The first 8-ft-diameter seamless test article tested as part of SBKF

I. Introduction

The NASA Engineering Safety Center (NESC) Shell Buckling Knockdown Factor Project (SBKF) was established in 2007 by the NESC with the primary objective to develop *analysis-based* buckling design factors and guidelines for metallic and composite launch-vehicle structures.[1] A secondary objective of the project is to advance technologies that have the potential to increase the structural efficiency of launch-vehicles. The SBKF Project has determined that weld-land stiffness discontinuities can significantly reduce the buckling load of a cylinder. In addition, the welding

[1] Aerospace Engineer, Dynamics, Loads & Strength Branch, EV31, Member AIAA.
[2] Senior Research Engineer, Structural Mechanics & Concepts Branch, MS 190, Senior Member AIAA.
[3] Research Aerospace Engineer, Structural Mechanics & Concepts Branch, MS 190, Associate Fellow AIAA.
[4] Senior Structural Analyst, Structural and Thermal Systems Branch, MS 431, AIAA Senior Member
[5] Senior Scientist, supporting the Structural Mechanics & Concepts Branch, MS 190.
[6] Research Aerospace Engineer, Structural Mechanics & Concepts Branch, MS 190, Senior Member AIAA.

process can introduce localized geometric imperfections that can further exacerbate the inherent buckling imperfection sensitivity of the cylinder. Therefore, single-piece barrel fabrication technologies can improve structural efficiency by eliminating these weld-land issues.

As part of this effort, SBKF partnered with the Advanced Materials and Processing Branch (AMPB) at NASA Langley Research Center (LaRC), the Mechanical and Fabrication Branch at NASA Marshall Space Flight Center (MSFC), and ATI Forged Products to design and fabricate an 8-ft-diameter orthogrid-stiffened seamless metallic cylinder. The cylinder was subjected to seven subcritical load sequences (load levels that are not intended to induce test article buckling or material failure) and one load sequence to failure. The purpose of this test effort was to demonstrate the potential benefits of building cylindrical structures with no weld lands using the flow-formed manufacturing process. This seamless barrel is the ninth 8-ft-diameter metallic barrel and the first single-piece metallic structure to be tested under this program.

II. Testing Details

A. Test Facility

The testing was conducted at MSFC in a test assembly (Figure 1) that was designed, analytically verified, and fabricated to meet program test objectives. The test assembly is a self-reacting load system composed of an upper and lower load spider, 16 load struts, upper and lower transition sections, the test-article assembly, and eight load lines. Each load line consists of a hydraulic cylinder, 4-in.-diameter loading rod, a load cell, and attachment hardware. The load lines can be controlled independently in load control or position control to apply uniform compression or tension, or combined axial and bending loads with a maximum load capability of 1,500,000 lb of axial compression force and 80,000 lb of axial tension.

B. Test Article

The test article, also referred to as STA8.1, was manufactured from an 8,000 pound Al-2219 ingot at ATI Forged Products using a flow-forming process to produce a cylinder with an outside diameter of 96 in., a length of 90 in., and a wall thickness of 2.5 inches. The cylinder was then heat treated to reach its final Al 2219- T851 condition. From the 90 in., a total of 10 in. was removed from the forward and aft ends for material property testing, which confirmed that the flow-forming process produced material properties were representative of Al 2219-T851 plate properties defined in the Metallic Materials Properties Development and Standardization (MMPDS) [2].

The cylinder was then shipped to MSFC where the outer mold line (OML) was milled to its final diameter. The orthogrid pattern was then milled on the inside surface of the cylinder using a 7-axis milling machine, as shown in Figure 2. To perform stiffener milling, the cylinder was laid on its side and secured in place using a custom vacuum chuck. The stiffener pattern was machined in three arc segments. Since there were no weld lands, 145 longitudinal stiffeners are evenly spaced at 2.482 degrees around the circumference of the barrel, and the circumferential ribs have a spacing of 5.064 in.. The longitudinal and circumferential stiffeners have the same thickness of 0.065 in. The stiffener height is 0.570 in. as measured from the OML, and the skin thickness is 0.070 in. After the orthogrid pattern was machined, the barrel was machined to its final height of 77.595 in. Next, the barrel was bolted and potted into steel interface rings, and prior to being installed in the test fixture, the barrel was structured-light scanned to obtain the geometric imperfections, which are shown in Figure 3.

III. Test-Analysis Correlation

A. Pretest Predictions

The finite-element analysis was performed using the general-purpose finite-element analysis code, Abaqus 2016[3]. The barrel was modeled using S4R reduced-integration four-noded elements; see Figure 4 for mesh density details. To accurately model the load introduction into the test article, the entire test assembly was modeled using a combination of S4R shell and B31 beam elements (Figure 5). Point loads were applied at the ends of the eight load lines. The test assembly finite-element model contained 624,278 elements and 663,011 nodes.

Two models of STA8.1 were created: the first used nominal thicknesses with the measured geometric imperfections, and the second used an estimate of the as-built geometry thicknesses with the measured geometric imperfections. The as-built geometry, obtained during post-machining inspections, revealed variability in the shell-wall thickness. The as-designed nominal pocket thickness was 0.070 in., but the inspections reported the as-built pocket thickness varied from 0.071 in. to 0.081 in. Previous metallic barrel pocket measurements showed that the average pocket thicknesses were 0.003 in. thicker than specified on the drawings. Therefore, a skin thickness of 0.073 in. was used in the as-built-geometry analysis. See Table 1 for nominal thickness and modeled thicknesses. Though

this increased thickness is still within tolerances specified on the drawing, it had a significant effect on the predicted buckling load. These effects of the as-built geometry on the pretest predictions will be discussed in the proposed paper. The as-built geometry model predicted a buckling load of 725,000 lb, and the predictions presented in this abstract are from the analysis with the as-built geometry.

B. Test Results

To validate the finite-element model prior to the test to failure, seven subcritical tests were performed and the strain, displacement, and load data from the subcritical tests were plotted against the predictions. Three axial load sequences compressed the STA8.1 to 20%, 40% and 60% of the predicted linear-elastic buckling load of the geometrically perfect barrel with nominal geometry; and four combined bending and compression load sequences applied maximum compressive load in the 0^0, 90^0, 180^0, and 270^0 directions. The test article was highly instrumented with approximately 180 electrical-resistance strain gages and 24 displacement sensors. In addition, fiber-optic strain sensors, and low- and high-speed digital image correlation systems (DIC) were used to gather strain and displacement data.

The subcritical tests showed good qualitative and quantitative correlation with the predictions for all measured strains and displacements. The predicted and measured radial displacements at a load of 409,928 lb are presented in Figure 6. Both contour plots show very similar displacement patterns, eight full waves and one half wave, and similar displacement magnitudes.

During the final test to failure, the prebuckling response was very similar to that in the pure compression subcritical tests. Previously tested welded-metallic barrels had buckling events that originated at a single inward dimple, usually at the weld lands, which rapidly grew until the test article failed. Initial examination suggests there may not have been a single location where the buckling event initiated in STA8.1, but rather the test article exhibited a global collapse. Buckling occurred at 743,000 lb, within a 2.5% of the predicted 725,000 lb. The load versus axial displacement from the final load sequences is presented in Figure 8. Both Figures 7a and 7b present the radial contour plots at buckling from the analysis and the test. Instead of one notable location of inward displacement, represented by the dark blue color, there are multiple locations present at the maximum load that may have simultaneously led to the global buckling event. The radial displacement plots for Figures 6a and 6b and Figures 7a and 7b show characteristics of the first buckling eigenmode shape.

C. Posttest Correlation

As is seen in the load-end shortening curve from the final load sequence, Figure 8, the test article was stiffer than predicted even with the finite-element skin thicknesses adjusted to reflect the as-built geometry. According to the computer aided design (CAD) model, the weight of the barrel should be 265 lb, but the test article was measured to be 300 lb. The increased skin thickness in the as-built model geometry used in the pretest predictions only accounts for a fraction of this 35 lb difference. Therefore, it is possible that the average as-built measurements are greater than those used in the thickness-modified finite-element model. A detailed mapping of STA8.1's pocket thicknesses and stiffeners will be completed, and the finite-element model will be updated to reflect this new information. Additionally, it has been seen that including the fillets at the intersections of the stiffeners and the base of the stiffeners can increase the overall stiffness of the cylinder[4]. As-built pocket thicknesses and fillet features will also be addressed in the model refinements. Results from the refined model will be included in the proposed paper.

IV. Concluding Remarks

The design of welded metallic launch vehicles is heavily driven by the manufacturing process. The inclusion of weld lands and the welding process can introduce stiffness discontinuities which have a significant impact on the stability of the structure. To demonstrate the efficiency of structures with no weld lands, an 8-ft diameter orthogrid-stiffened cylinder, STA8.1, was tested to failure.

This test is the beginning of an on-going study to assess the benefits of seamless structures. A comparison of a previously tested welded-metallic barrel and the seamless barrel, as well as an in-depth analytical study assessing the benefits of this technology on large-scale launch vehicles will be documented in a future paper. This paper will only address the test and analysis correlation of STA8.1.

Overall, the predicated displacements and buckling load matched well with the test data; the predicted failure load was within 2.5% of the measured test load, and the predicted radial displacements prior to buckling and at buckling have good agreement with the measured radial displacements. The proposed paper will outline the test and analysis correlation for STA8.1, such as model refinements and sensitivity studies.

Acknowledgements

This work was conducted as part of the NASA Engineering and Safety Center (NESC) Shell Buckling Knockdown Factor Project, NESC assessment number 07-010-E. The barrel was flow formed by ATI Forged Products. The material properties were characterized by the Advanced Materials and Processing Branch at NASA Langley Research Center. The large-scale testing was performed by the Structural Strength Test Group (ET30) at MSFC.

References

[1]Hilburger M.W., "Developing the Next Generation Shell Buckling Design Factors and Technologies," *Proceedings of the 53rd AIAA/ASME/ASCE/AHS/ASC Structures, Structural Dynamics and Materials Conference*, AIAA paper no. 2012-1686, Honolulu, HI, April 2012.

[2]Anonymous, "Metallic Material Properties Development and Standardization," MMPDS-10, April 2015.

[3]Abaqus/Standard 2016, Software Package, SIMULIA, Rising Sun Mills, Providence, RI, 2016.

[4]Hilburger, M. W., Lindell, M. C. Lovejoy, A. E., Haynie, W. T., Waters, W. A., Jr., Gardner, N. W., and Matarese, R. A., "Buckling Analysis and Test Results from Selected 8-Foot-Diameter Integrally-Stiffened Al-Li Cylinder Test Articles", NASA TM-2017-000000, 2017. (In preparation)

Table 1. STA8.1 as-built geometry model inputs.

	Nominal	Modeled
Skin thickness	0.070 in.	0.073 in.
Stiffener height	0.500 in.	0.500 in.
Stiffener thickness	0.065 in.	0.066 in.
Transition thickness	0.135 in.	0.139 in.
End thickness	0.200 in.	0.206 in.

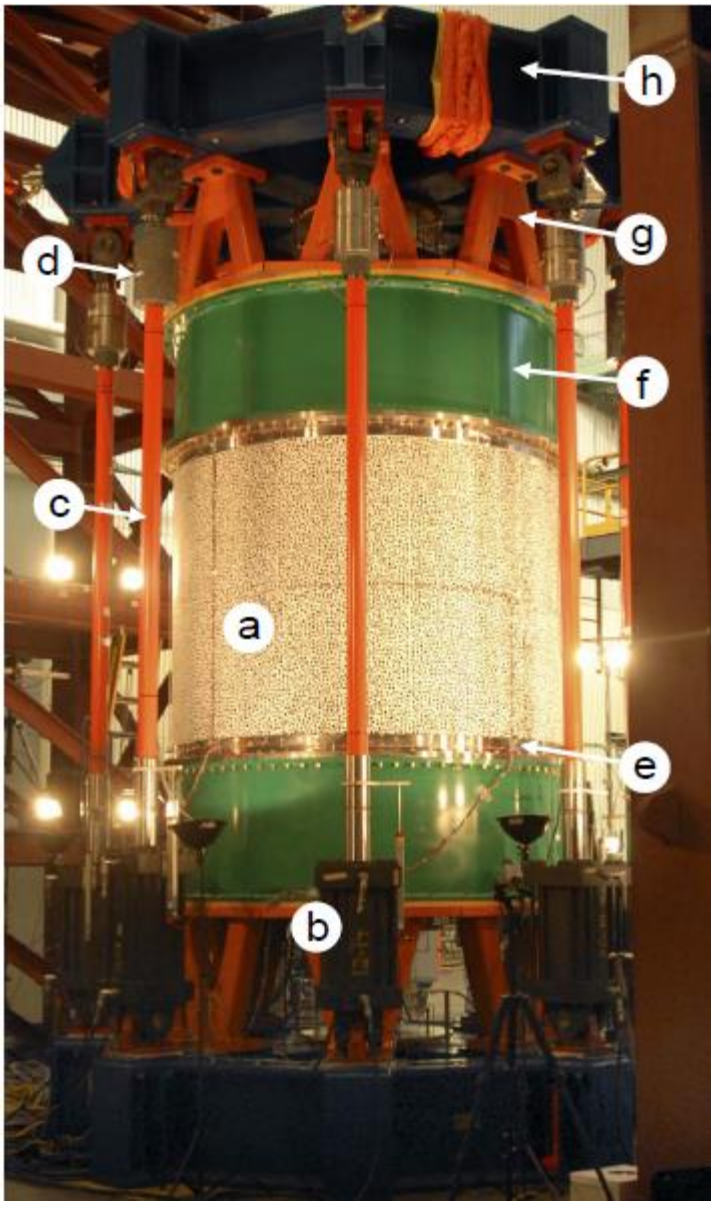

Figure 1. Eight-foot-diameter shell buckling test facility at MSFC: a) test article assembly, b) hydraulic actuator, c) loading rod, d) load cell, e) interface ring, f) transition section, g) load strut, and h) loading spider.

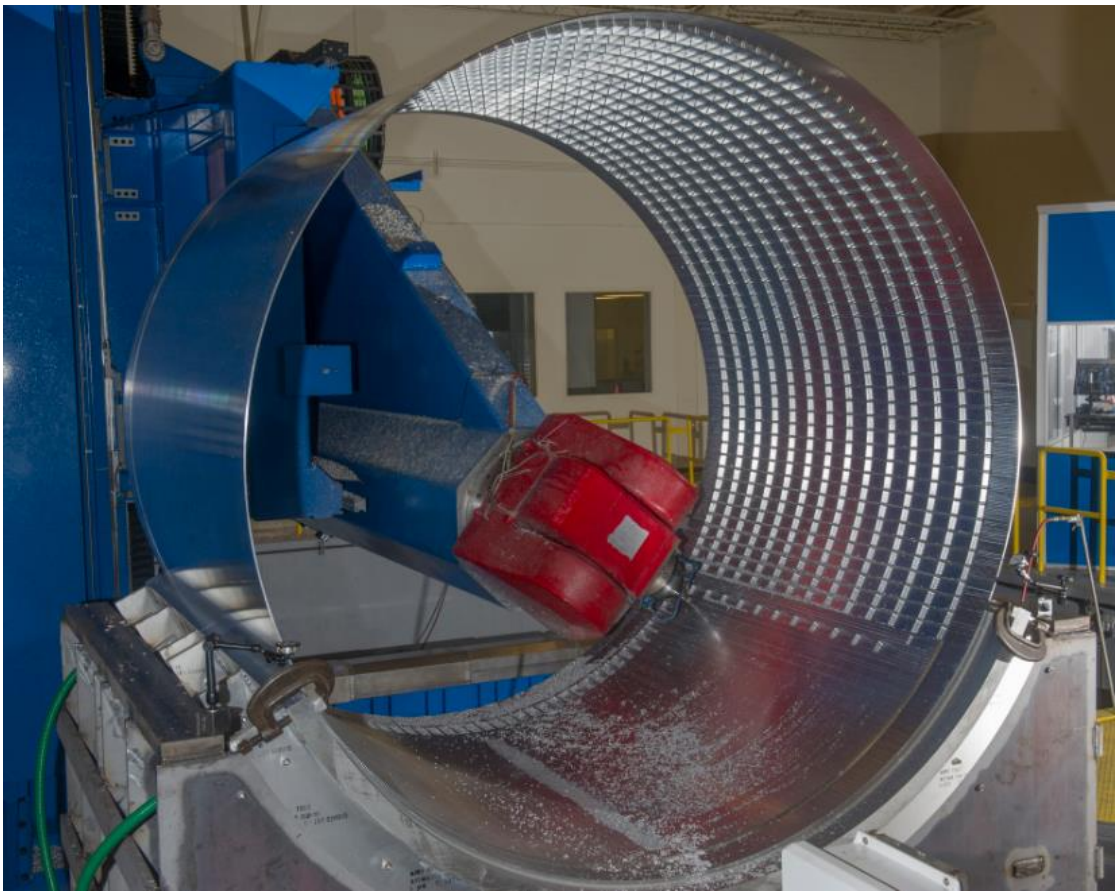

Figure 2. STA8.1 being machined on the 7-axis milling machine.

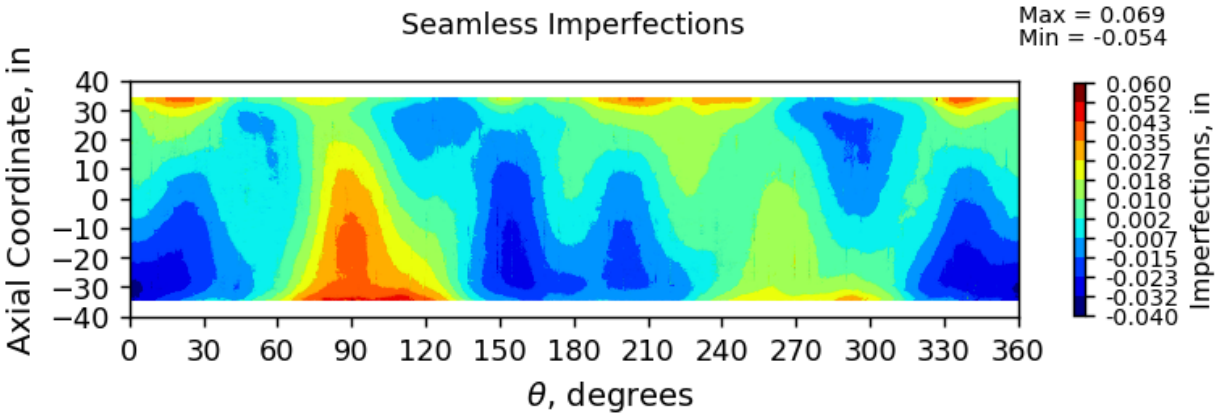

Figure 3. STA8.1 radial imperfections.

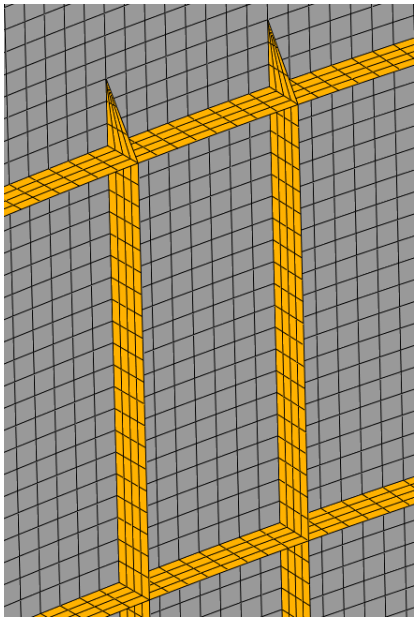

Figure 4. STA8.1 finite-element mesh detail.

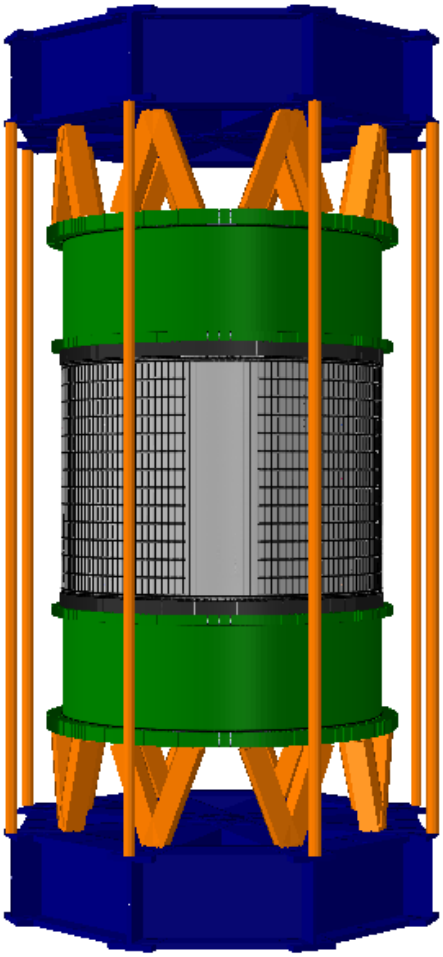

Figure 5. STA8.1 test assembly finite-element model.

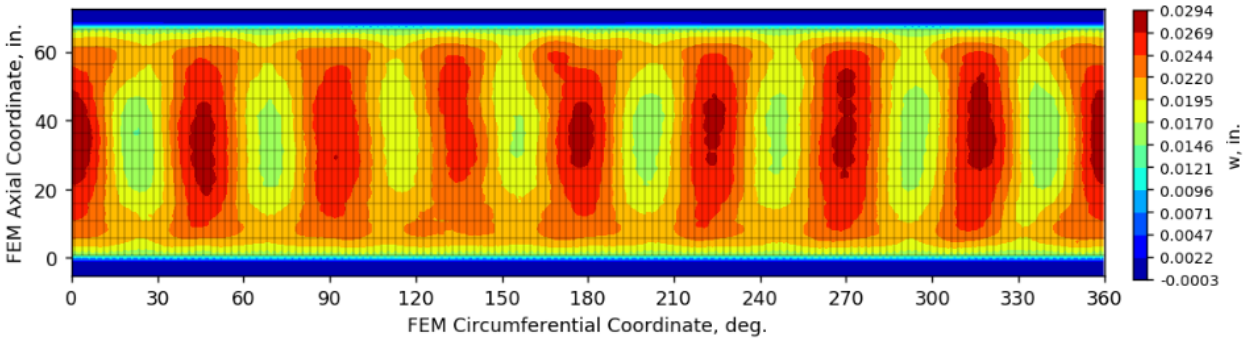

(a) Pretest prediction

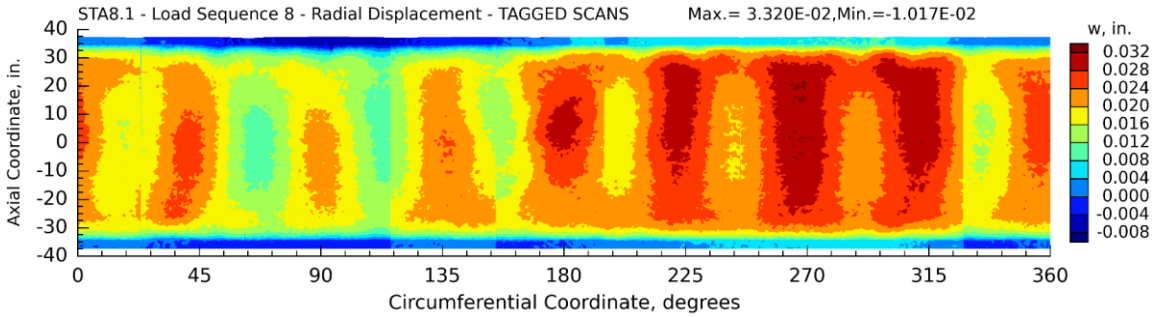

(b) Test

Figure 6. Radial displacement at 409,928 lb load.

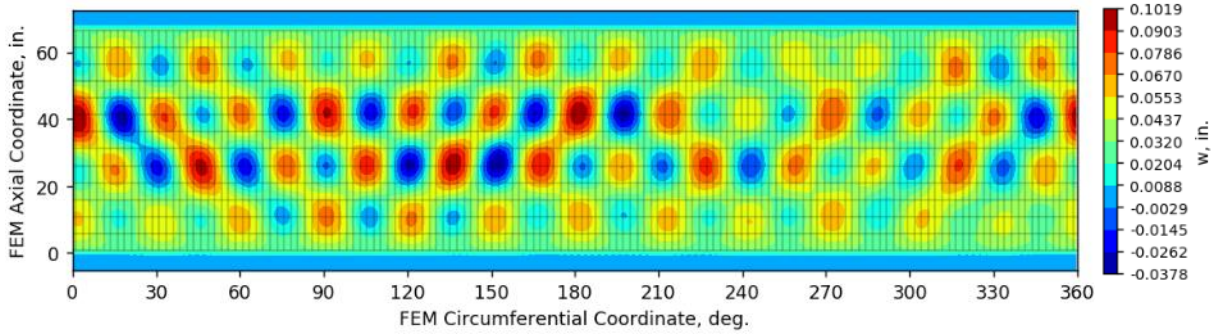

(a) Pretest prediction

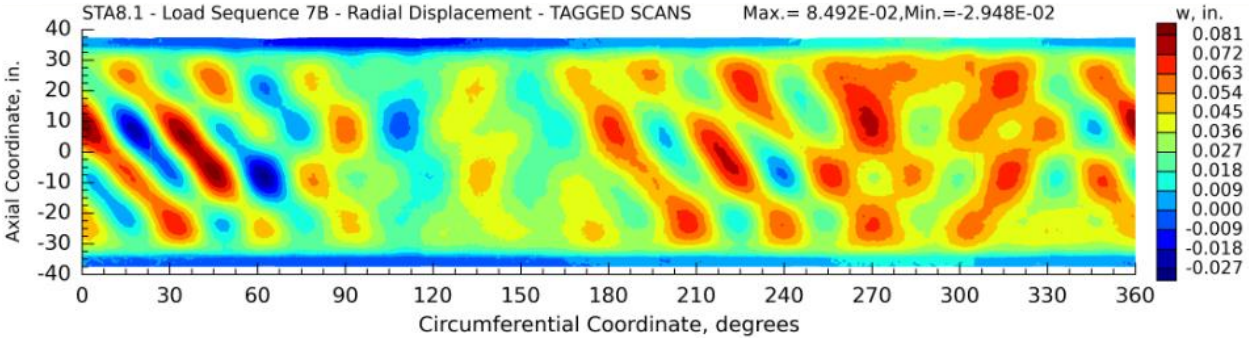

(b) Test

Figure 7. Radial displacement at buckling.

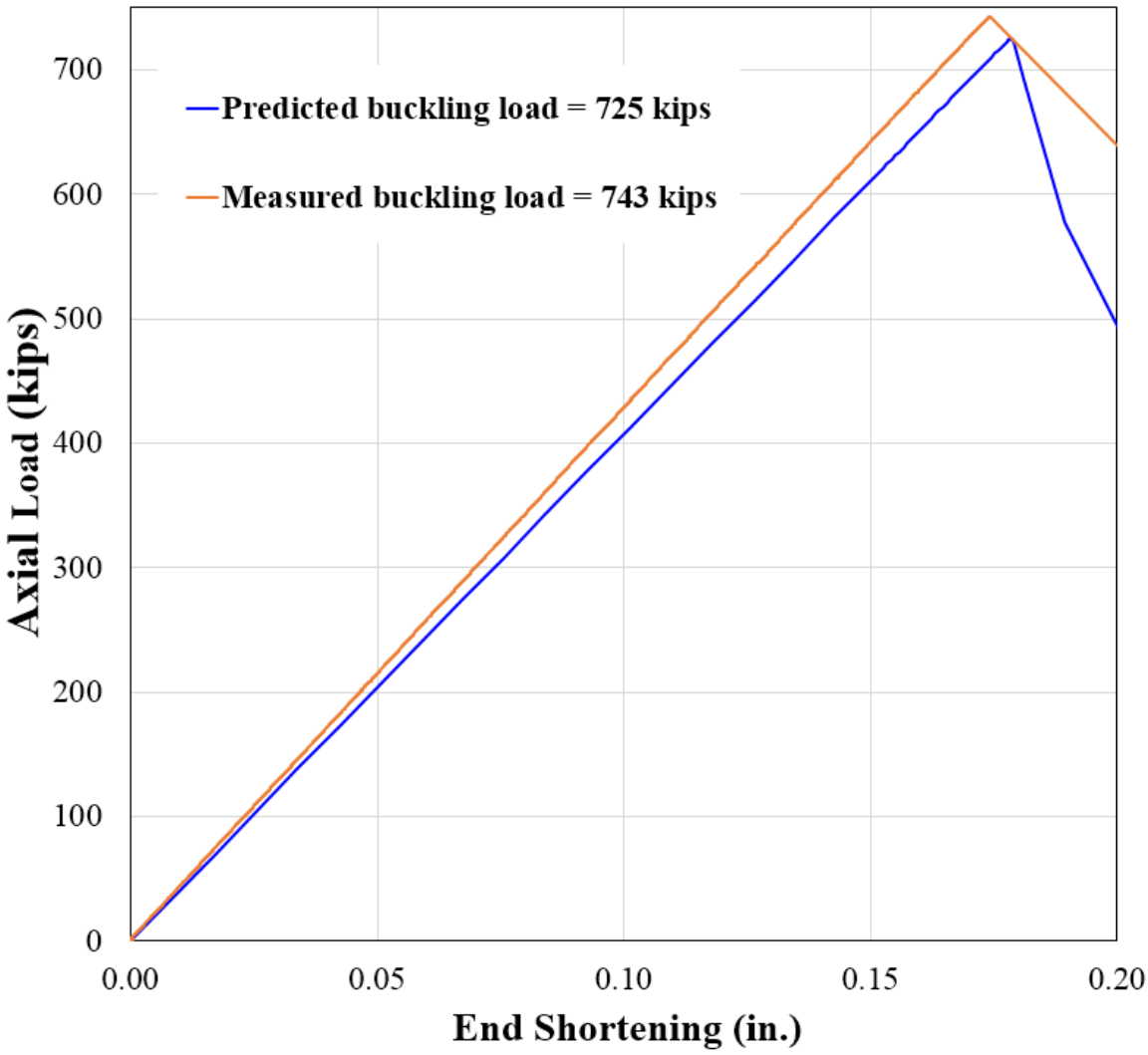

Figure 8. Load vs. average axial displacement for final load sequence.